Cement & Concrete Composites 36 (2013) 65–70

Contents lists available at SciVerse ScienceDirect

Cement & Concrete Composites

journal homepage: www.elsevier.com/locate/cemconcomp

# Nano-mechanical characterization of synthetic calcium–silicate–hydrate (C–S–H) with varying $CaO/SiO_2$ mixture ratios

Jung J. Kim [a], Emmy M. Foley [b], Mahmoud M. Reda Taha [c,*]

[a] Dept. of Civil and Environmental Engineering, Sejong University, Seoul, Republic of Korea
[b] Arizona Public Service, Winterburg, AZ 85354, United States
[c] Dept. of Civil Engineering, University of New Mexico, MSC01 1070, 1 University of New Mexico, Albuquerque, NM 87131-0001, United States

ARTICLE INFO

*Article history:*
Received 2 February 2012
Received in revised form 4 September 2012
Accepted 3 October 2012
Available online 23 October 2012

*Keywords:*
A. Drying
B. Calcium silicate hydrate (C–S–H)
C. Mechanical properties

ABSTRACT

Synthetic calcium silicate hydrate (C–S–H) made with calcium to silicate (C/S) mixture ratios of 0.9, 1.2 and 1.5 respectively is characterized. C–S–H was produced by extracting calcium oxide (CaO) from calcium carbonate ($CaCO_3$) and then mixing it with micro-silica ($SiO_2$) and deionized water to make slurry. The slurry was continuously mixed for 7 days, then the excess water was removed and thermo gravimetric analysis (TGA) was conducted. The drying method was equilibrated to 11% relative humidity (RH). The stoichiometric formula of the synthetic C–S–H were approximated as $C_{0.7}SH_{0.6}$, $C_{1.0}SH_{0.8}$ and $C_{1.2}SH_{2.4}$ for C/S mixture ratios of 0.9, 1.2 and 1.5 respectively. The dried powders were characterized using X-ray diffraction analysis (XRDA), and $^{29}Si$ magic angle spinning (MAS) nuclear magnetic resonance (NMR) spectroscopy. The powders were also compacted with 95 MPa pressure and nanoindentation of the compacted specimens were then undergone to mechanically characterize the synthetic C–S–H. The experiments provide insight on the nanoscale mechanical characteristics of C–S–H.

© 2012 Elsevier Ltd. All rights reserved.

## 1. Introduction

As calcium silicate hydrate (C–S–H) makes up about 67% of hydrated Portland cement paste [1], it is essential to interpret C–S–H structure and characteristics for desirable properties of cement hydration products and thus macroscale concrete. Researchers have reported many efforts to study C–S–H [2–5]. C–S–H was synthesized by mixing aqueous solutions of sodium metasilicate and calcium oxide with various ratios [2]. Using the compacted C–S–H discs supported by three points, the modulus of elasticity was measured. By mixing calcium oxide with either silicic acid or silica fume and distilled water, C–S–H was synthesized with C/S ratios ranging between 0.9 and 1.7 [3]. The solubility of the C–S–H was tested. At C/S ratios of 0.65, 0.83, 0.90, 1.10, and 1.20 by mixing calcium oxide with amorphous silica and distilled water, C–S–H was synthesized [4]. The durability of the C–S–H against leaching in sodium chloride solution was tested. Synthesized C–S–H by mixing amorphous silica with calcium oxide in excess water was used for mechanical characterizations of beam-like specimens [5].

Standard drying techniques to cement and C–S–H samples were employed to achieve standard water contents for experimental repeatability. Type I Portland cement was hydrated for 1.5 years in a bottle at a water to cement ratio (w/c) of 0.5 [6]. The hydrated cement was then dried to 11% relative humidity (RH). Recently, it was also reported that at 11% RH, only a monolayer of adsorbed water exists on the surface of the particles in addition to the interlayer water. This surface water aids in compaction of the C–S–H powder [5].

Nanoindentation experiments of cement pastes have shown that outer and inner product C–S–H can be categorized as low density (LD) and high density (HD) C–S–H [7,8]. It was shown that the low-stiffness phase of LD C–S–H makes up around 67% of the C–S–H present in the paste, with an elastic modulus of 21.7 ± 2.2 GPa. On the other hand, the high-stiffness phase of HD C–S–H makes up the remaining 33% of the C–S–H and has an elastic modulus of 29.4 ± 2.4 GPa. Nanoindentation tests were also performed on a low w/c ultra high performance concrete (UHPC) [9]. According to the study, C–S–H with a C/S ratio of less than 1.0 has an elastic modulus of 20.0 ± 2.0 GPa and C–S–H with a C/S ratio of greater than 1.0 has an elastic modulus of 31.0 ± 4.0 GPa. Mondal et al. [10] reported a value of 23.0 GPa for elastic modulus of C–S–H in the middle of the cement paste matrix, far from unhydrated particles. When indenting C–S–H gel close to unhydrated cement particles, elastic modulus of C–S–H ranging between 1.3 and 40.0 GPa was found [10].

In this study, C–S–H is synthesized with a C/S mixture ratio of 0.9, 1.2 and 1.5 respectively. C–S–H is then chemically and mechanically characterized. C–S–H powder was dried to equilibrate 11% RH and was then mechanically characterized using nanoindentation.

* Corresponding author. Tel.: +1 505 277 1258; fax: +1 505 277 1988.
*E-mail address:* mrtaha@unm.edu (M.M. Reda Taha).

0958-9465/$ - see front matter © 2012 Elsevier Ltd. All rights reserved.
http://dx.doi.org/10.1016/j.cemconcomp.2012.10.001

## 2. Experimental study

### 2.1. Synthesis of C–S–H

Reagent grade calcium carbonate ($CaCO_3$) from Mallinckrodt Chemicals was used to make lime (CaO) for the C–S–H. The purity of 99.7% of $CaCO_3$ was confirmed by thermo gravimetric analysis (TGA). Fumed silica from Aldrich with 99.8% purity was used for the silicate portion of the C–S–H. Deionized water was used for mixing. C–S–H was synthesized by calcining $CaCO_3$ into CaO by heating to 900 °C for 24 h. Once pure lime was obtained, it was removed from the furnace and placed under nitrogen to prevent carbonation. The lime was then mixed with fumed silica at varying C/S mixture ratios, respectively, and enough deionized water to produce slurries. The slurries were continuously mixed for 7 days to allow complete reaction. The excess water was filtered off using vacuum after mixing. A standard drying method to achieve 11% RH was used.

The standard drying method employed was equilibration to 11% RH using saturated lithium chloride (LiCl) [11]. This method has been used by many researchers [12,13]. The salt solution was prepared following ASTM Standard E 104-02 [14]. The system was set up as a series of three beakers as shown in Fig. 1. The first beaker contained the saturated LiCl solution, which was put on a hot plate on the lowest setting to keep the ambient temperature in the beaker constant. The second beaker contained the C–S–H, and the third contained drierite (calcium sulfate and cobalt chloride) to catch the excess water before it reached the vacuum pump. The third beaker was connected directly to the vacuum source. The C–S–H was placed in the system while under a Nitrogen environment. The drying process continued until a change in mass of less than 0.1% per day was observed. Furthermore standard D-Drying method [11] was performed on a few samples to examine the significance of water content on C–S–H compaction. Details on the D-Drying process can be found elsewhere [11].

### 2.2. Chemical characterization of C–S–H

#### 2.2.1. Thermo gravimetric analysis (TGA)

From 25 °C to 1000 °C, heated at 10 °C/min, TGA tests were performed. As the TGA test is useful for estimating calcium hydroxide (CH) and calcium carbonate contents, it was used for estimating the stoichiometric formula of the synthetic C–S–H. In this study, we observed a similar temperature range to that reported by Jain and Neithalath [15]. TGA tests were performed on C–S–H slurries without standard drying. As these slurries of the synthetic C–S–H for TGA include an arbitrary amount of water, the initial mass is taken as the mass of the sample at 145 °C. The mass loss at the temperature range between 145 °C and 350 °C denoted as $\%mL_1$ is then considered as the loss of water from C–S–H. The mass loss at the temperature range between 350 °C and 500 °C denoted as $\%mL_2$ is considered as the loss of water from CH, while that at the temperature range between 600 °C and 825 °C denoted as $\%mL_3$ is considered as the loss of carbon dioxide ($CO_2$) from $CaCO_3$. After determining the contents of CH and $CaCO_3$, the remaining is considered as C–S–H. For the stoichiometric formula of C–S–H as $(CaO)_{C/S}\cdot(SiO_2)\cdot(H_2O)_x$, C/S ratio and the amount of water ($H_2O$) denoted "$x$" can be found for a given C/S mixture ratio of $\overline{C/S}$ as:

$$C/S = \frac{\overline{C/S}(100 - \%mL_1 - 4.113\%mL_2 - 2.274\%mL_3) - 3.336\%mL_2}{100 - \%mL_1 - \%mL_2 - 2.274\%mL_3} \quad (1)$$

$$x = \frac{\%mL_1(3.115\overline{C/S} + 3.337)}{100 - \%mL_1 - \%mL_2 - 2.274\%mL_3} \quad (2)$$

Eqs. (1) and (2) are derived from mass balances with the assumption that when the initial C/S mixture ratio of $\overline{C/S}$ is mixed with enough water, 1 mol of C–S–H and ($\overline{C/S}$–C/S) mol of CH will be synthesized. The consumption of CaO for $CaCO_3$ is neglected. %CSH is estimated as 100%–(%CH + %$CaCO_3$). %CH and %$CaCO_3$ are determined from $\%mL_2$ and $\%mL_3$ respectively by mass balance. The molecular weights of water, CH, $CO_2$, $CaCO_3$ and C–S–H as 18.01 g/mol, 74.1 g/mol, 44.01 g/mol, 100.09 g/mol and 56.1(C/S) + 60.1 + (18.01)$x$ g/mol are used for the derivation of Eqs. (1) and (2).

#### 2.2.2. X-ray diffraction analysis (XRDA)

X-ray diffraction (XRD) tests were performed on synthetic C–S–H powder after drying to 11% RH. Since C–S–H is very amorphous and weakly crystalline, it does not produce strong XRD peaks. For all synthetic C–S–H at varying C/S mixture ratios, the XRD peaks attributable to C–S–H were compared with published results [15].

#### 2.2.3. $^{29}$Si magic angle spinning (MAS) nuclear magnetic resonance (NMR)

$^{29}$Si MAS NMR spectroscopy was performed in 7 mm cylinders spun at 4 kHz. Approximately 10,000 scans were performed on each sample. $^{29}$Si NMR spectroscopy was performed on a Bruker ASX 300 spectrometer (7.05 T magnetic field) at 59.6 MHz. Single pulse experiments without $^1$H decoupling were carried out. The $^{29}$Si chemical shifts are respectively referenced relative to tetramethylsilane $Si(CH_3)_4$ (TMS) at 0 ppm, using $Si[(CH_3)_3]_8Si_8O_{20}$ (Q8M8) as a secondary reference (the major peak being at 11.6 ppm relatively to TMS). $^{29}$Si MAS NMR tests were performed on synthetic C–S–H powder after drying to 11% RH. A silicate tetrahedron having $n$ shared oxygen atoms is expressed as $Q^n$ where $n$ is the number oxygen atoms from 0 to 4. The intensity of the silicate $Q$ connections can be investigated using $^{29}$Si MAS NMR. For

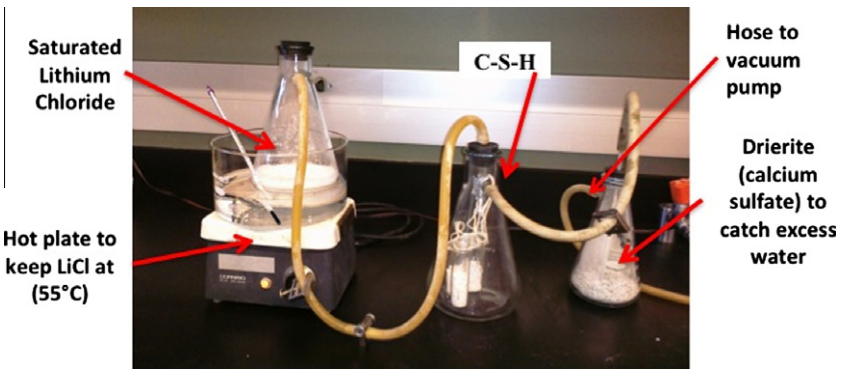


**Fig. 1.** Set-up of 11% relative humidity conditioning [11].

hydrated cement, the most common observed chains are $Q^1$ and $Q^2$, which resonate near −79.5 ppm and −85.3 ppm respectively [16]. Using the calculated intensity fractions of $Q^n$s, the average degree of C–S–H connectivity $n_c$ is calculated after Saoût et al. [17] as:

$$n_c = \frac{Q^1 + 2Q^2 + 3Q^3}{Q^1 + Q^2 + Q^3} \quad (3)$$

High value of $n_c$ represents high polymerization of C–S–H. The mean chain length $L$ is the number of silicates bound together in a chain and this is typically found using $Q^2/Q^1$ ratio as:

$$L = 2(1 + Q^2/Q^1) \quad (4)$$

The mean chain length $L$ is the number of silicates bound together in a chain and this is typically found using the $Q^2/Q^1$ ratio. Taylor [18] examined the chain lengths of naturally occurring calcium silicate hydrates in jennite and tobermorite. Jennite has a basic formula of $C_9S_6H_{11}$ (C/S = 1.5) and tobermorite has a basic formula of $C_5S_6H_5$ (C/S = 0.83) [18]. For these particular formula, the chain lengths are theoretically infinite. When some chains are missing some of the silica tetrahedra bridging the groups together, finite chain lengths exist.

### 2.3. Mechanical characterization of C–S–H

#### 2.3.1. Compaction

All C–S–H powder preparation was performed in a dry box filled with nitrogen to eliminate any chance of C–S–H contamination. Compaction was performed on synthetic C–S–H powder after drying to 11% RH using a hollow steel cylinder with a 31.75 mm inner diameter, two solid steel pistons 31 mm in diameter, one steel screen to allow relief of any excess pressure, one solid steel disc that fit the cylinder slightly tighter than the pistons to keep material from falling out and to create a smooth surface on one side, and one filter paper. 4.5 g of powder was used for each compaction, which was placed in the cylinder and steel pistons were placed on either side while under nitrogen to avoid specimen contact with $CO_2$. This cylinder was then sealed and placed in the compression machine for compaction. Nitrogen was not maintained during the compaction process. The dry box, the compaction cylinder and the compaction process are shown in Fig. 2. The load was applied under constant load rate of 1% maximum load per second and held at maximum load for 4 min before unloading. 10 discs of each type of C–S–H at varying C/S mixture ratios were made using 95 MPa pressure. The specimens were extracted from the cylinder under nitrogen and kept under nitrogen until additional testing.

#### 2.3.2. Nanoindentation

Specimens were prepared for nanoindentation by first casting them in acrylic to keep the specimens in place and to fit them into the nanoindentation holder. The specimens were then polished on a Buehler Ecomet 3 polisher with a Buehler Automet 2 power head, which applied a constant pressure to the specimens and provided additional spin on the specimens for increased polishing efficiency. The steps used during polishing were: 10 min with a 125-μm diamond pad, 15 min with a 70-μm diamond pad, 15 min with a 30-μm diamond pad, 30 min with a 9-μm diamond lapping film pad, and 1 h with a 1-μm diamond lapping film pad. All pads were lubricated with lapping oil to keep pads cool and to disperse removed material. The specimens were sonicated in ethanol in between grits. Nanoindentation was performed using a diamond Berkovich tip loaded at 0.55 mN including 0.05 mN preloading. A dwell period of 60 s was used at maximum load to account for thermal drift and creep. Nanoindentation was performed using NanoTest® system by Micro Materials. Thirty points were indented on each specimen and the results were analyzed to identify the submicron phases of C–S–H and their mechanical characteristics. Three discs were nanoindented after the powder being dried to standard 11% relative humidity then compacted at 95 MPa as described above for varying C/S mixture ratios.

## 3. Results and discussion

TGA curves for the synthetic C–S–H with C/S mixture ratio of 0.9, 1.2 and 1.5 are shown in Fig. 3 and the results are presented in Table 1. To exclude an additional absorbing water prior to performing the TGA from the TGA results, the initial weight is taken at 145 °C and presented in Fig. 3. The results in Table 1 showed that 88.8% C–S–H in the slurry synthesized with C/S mixture ratio of 0.9, with the balance being composed of 10.2% CH and 1% $CaCO_3$. In the slurry synthesized with C/S mixture ratio of 1.2, 88.5% C–S–H with the balance being composed of 10.3% CH and 1.2% $CaCO_3$ while 88.0% C–S–H with the balance being composed of 9.6% CH and 2.4% $CaCO_3$ in the slurry synthesized with C/S mixture ratio of 1.5. Using Eqs. (1) and (2) with the corresponding C/S mixture ratio, the value C/S and $x$ can be determined. The stoichiometric formulas of synthetic C–S–H dried to 11% RH in this study

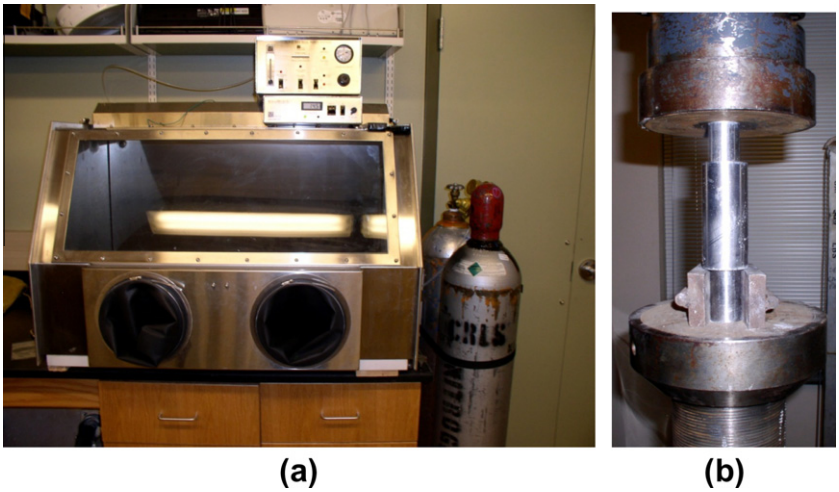


**Fig. 2.** Preparation of C–S–H discs using (a) dry box under Nitrogen environment. (b) cylinders and compaction process to produce C–S–H discs.

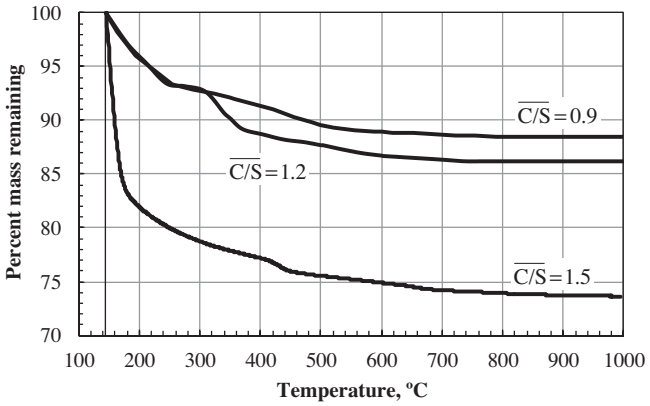


**Fig. 3.** TGA curves for C–S–H made with 0.9, 1.2 and 1.5 C/S mixture.

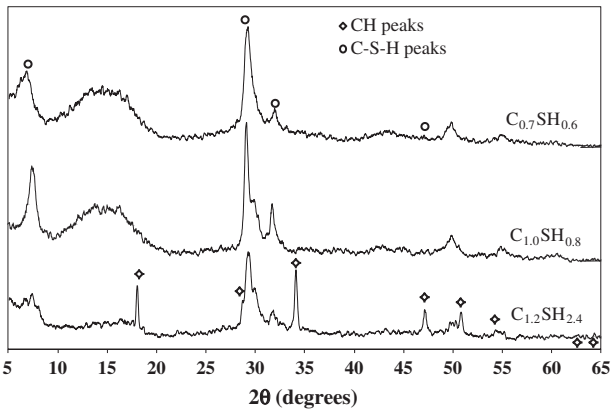


**Fig. 4.** XRDA spectrum of C–S–H. Peaks present at 29°, 32°, 7°, and 48° are characteristic of C–S–H. The slim peaks present at 18° and 34° indicate CH present in the specimen.

are approximated as $C_{0.7}SH_{0.6}$, $C_{1.0}SH_{0.8}$ and $C_{1.2}SH_{2.4}$ for C/S mixture ratios 0.9, 1.2 and 1.5 respectively.

The XRDA of C–S–H showed several phases of C–S–H as well as some CH and $CaCO_3$ as shown in Fig. 4. The XRDA spectrum of $C_{1.2}SH_{2.4}$ showed several phases of C–S–H mixed with some CH. Since CH is much more crystalline than C–S–H and XRD peaks are produced by X-ray beams diffracting of crystals, CH peaks show up disproportionately high for their actual volume in the sample. The XRD peaks attributable to C–S–H at 7°, 29°, 32° and 48° lined up well with published results [15]. The slim peaks present at 18° and 34° indicate CH present in the sample. It is very difficult to determine with certainty if $CaCO_3$ is present, as the strongest peak would appear around 29.5°, coincident with peaks of C–S–H. The other peaks representative of $CaCO_3$ are so weak that they could easily be lost in the background noise of the spectra. XRD analysis of $C_{0.7}SH_{0.6}$ and $C_{1.0}SH_{0.8}$ showed only peaks for C–S–H with no CH present. Peaks observed also match well with published results for C–S–H [15].

NMR spectra of each type of C–S–H are shown in Fig. 5. Statistical deconvolution analysis as performed on NMR results and presented in Table 2. The peaks of −79, −82.6 and −85 ppm for $Q^1$, $Q_b^2$ and $Q^2$ silicate connections are used for deconvolution analyses of NMR spectra respectively [17]. The standard deviations of 1.0–1.54 ppm are assigned to the normal distributions of $Q^1$, $Q_b^2$ and $Q^2$. The deconvoluted peaks are also shown in Fig. 5. The slight shifts of $Q^1$ and $Q^2$ peaks for $C_{0.7}SH_{0.6}$ to more negative chemical shift than $C_{1.2}SH_{2.4}$ might indicate the increase in the degree of the silicate polymerization [19]. As C/S ratio decreases, there is an obvious change in the $Q^2/Q^1$ ratio as presented in Table 2. Only a slight change in the $Q^2/Q^1$ ratio is observed when the C/S ratio drops from 1.2 to 1.0. However, a very substantial increase in polymerization of the silica indicated by an increase of $Q^2$ bond was observed and $Q_b^2$ bond appears when the C/S ratio was dropped to 0.7. These results are similar to those observed by other researchers [16,20] and further prove the formation of C–S–H. The degree of polymerization $n_c$ and the mean chain length $L$ for $C_{0.7}SH_{0.6}$, $C_{1.0}SH_{0.8}$ and $C_{1.2}SH_{2.4}$ are calculated using Eqs. (3) and (4), respectively, and presented in Table 2. As a reference for scale, the maximum C-S-H polymerization, 100% $Q^3$ bond, would have a

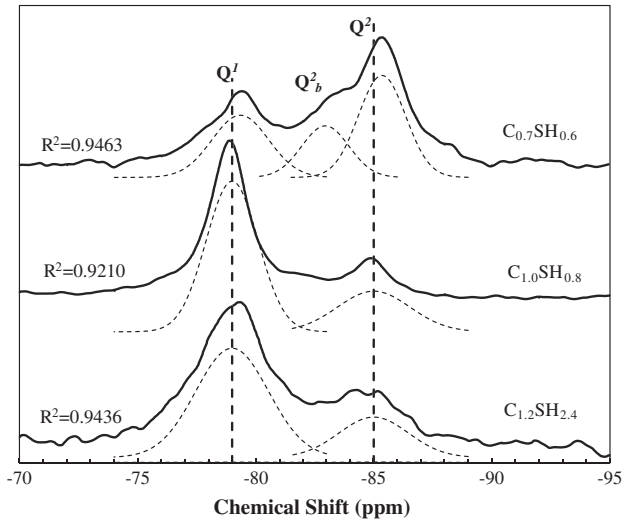


**Fig. 5.** $^{29}Si$ NMR Spectra of C–S–H, $R^2 > 0.92$.

polymerization value of 3 while 100% $Q^1$ bond would have a polymerization value of 1. Chain lengths observed are not similar at all to jennite but are somewhat similar to lengths reported for tobermorite. Jennite is reported to have an almost infinite chain length at C/S ratios of 1.2 and 0.9, while tobermorite has chain lengths of 2.3 and 11 for 1.2 and 0.9 C/S ratios respectively [18]. These observations confirm that low C/S ratios might favor forming tobermorite-like C–S–H.

Nanoindentation results and the deconvolution analyses of elastic modulus are presented in Fig. 6 and Table 3. For the specimen compacted to 95 MPa, the deconvolution analysis of elastic modulus for C–S–H gives three ranges of Young's modulus values: 1.2–15.4, 17.1–32.0 and over 40.0 GPa. From knowledge of the properties of CH and TGA results showing CH content in the synthetic C–S–H slurry, materials with elastic modulus higher or equal

**Table 1**
Synthetic C–S–H slurry compositions from TGA analysis results and the stoichiometric formula of the synthetic C–S–H estimated from TGA results.

| $\overline{C/S}$ | Mass loss (145–350 °C) (%) | C/S | $x$ | Mass loss (350–500 °C) (%) | CH content (%) | Mass loss (600–825 °C) (%) | $CaCO_3$ content (%) |
|---|---|---|---|---|---|---|---|
| 0.9 | 7.895 | 0.73 | 0.55 | 2.486 | 10.2 | 0.443 | 1.0 |
| 1.2 | 9.81 | 1.0 | 0.8 | 2.503 | 10.3 | 0.527 | 1.2 |
| 1.5 | 22.12 | 1.24 | 2.42 | 2.334 | 9.6 | 1.035 | 2.4 |

**Table 2**
Integration of $Q^n$ intensities by deconvolution of $^{29}$Si MAS NMR spectra.

| C–S–H formula | $Q^1$ | $Q_b^2$ | $Q^2$ | $Q^2/Q^1$ | $n_c$ | $L$ |
|---|---|---|---|---|---|---|
| $C_{0.7}SH_{0.6}$ | 0.327 | 0.226 | 0.447 | 2.06 | 1.673 | 6.11 |
| $C_{1.0}SH_{0.8}$ | 0.726 | – | 0.274 | 0.38 | 1.274 | 2.75 |
| $C_{1.2}SH_{2.4}$ | 0.739 | – | 0.261 | 0.36 | 1.262 | 2.72 |

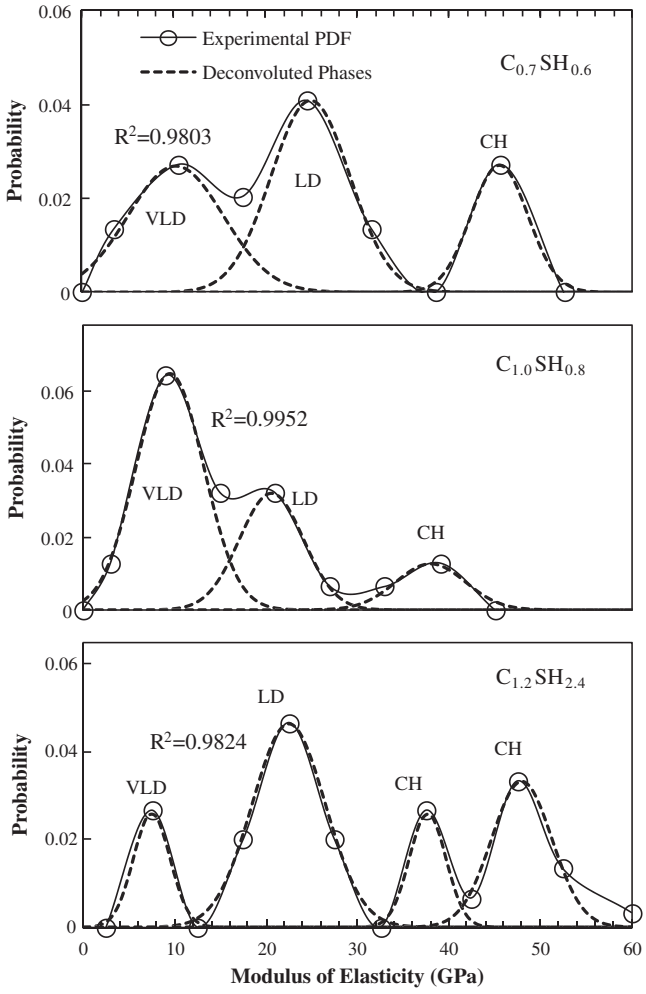


**Fig. 6.** Deconvolution analyses of nanoindentation results, $R^2 > 0.94$.

to 45 GPa are believed to be CH and are therefore excluded when calculating C–S–H mechanical characteristics. The relative

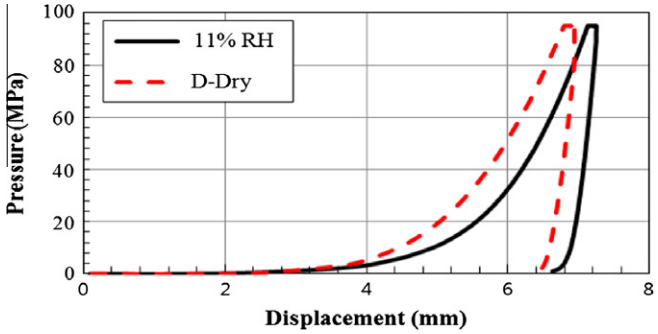


**Fig. 7.** Comparison of the compaction curves of D-Dry versus 11%RH cured C–S–H showing higher compactability of 11% RH cured C–S–H compared with D-Dry cured C–S–H.

fractions of Young's modulus ranges of 1.2–15.4 GPa and 17.1–32.0 GPa are presented in Table 3. The weighted averages of the compacted C–S–H discs elastic modulus were 18.4 GPa, 13.0 GPa and 19.2 GPa for as $C_{0.7}SH_{0.6}$, $C_{1.0}SH_{0.8}$ and $C_{1.2}SH_{2.4}$ respectively. Other methods such as the homogenization technique to compute the modulus of elasticity of the composite C–S–H might yield more accurate results than the weighted average method. Details on the homogenization method can be found elsewhere [21].

While the elastic modulus of the compacted discs for $C_{0.7}SH_{0.6}$ and $C_{1.2}SH_{2.4}$ are in line with published elastic modulus values putting it into the category of LD C–S–H [8], the elastic modulus of the compacted disc for $C_{1.0}SH_{0.8}$ is much less than that of LD C–S–H. It seems that the higher modulus of $C_{1.2}SH_{2.4}$ than that of $C_{1.0}SH_{0.8}$ is most likely due to higher water content of $C_{1.2}SH_{2.4}$ than that of $C_{1.0}SH_{0.8}$. This might be attributed to the role of water to improve compaction. Analysis of the compaction curves of C–S–H under two drying conditions (11% RH) and D-Dry (7% RH) [11] showed that C–S–H with 11% RH was easier to compact than the D-Dry cured C–S–H as shown in Fig. 7. Analysis of the unloading parts of the compaction curves showed that the compacted C–S–H had a modulus of elasticity of 9.5 GPa for 11% RH cured C–S–H compared with 8.9 GPa for D-Dry cured C–S–H proving the role of water on improving C–S–H compaction.

The relatively high modulus of $C_{0.7}SH_{0.6}$, in spite of its relatively low water content, might be attributed to the relatively high polymerization of $C_{0.7}SH_{0.6}$ compared with $C_{1.0}SH_{0.8}$. While a full explanation of that observation needs further in-depth investigations and more replication of these tests, we offer a possible explanation as the modulus of C–S–H is associated to not only its porosity considering granular nature but also its silicate polymerization which might increase 'glubule' modulus consisting C–S–H [12]. Further research is needed to confirm or negate this suggestion.

**Table 3**
Surface fractions from nanoindentation results of the C–S–H discs compacted with 95 MPa pressure according to Young's modulus of elasticity.

| C–S–H formula | C–S–H phase categorization | Surface fraction (%) | Young's modulus (GPa) | C–S–H weighted average (GPa) |
|---|---|---|---|---|
| $C_{0.7}SH_{0.6}$ | VLD | 35 | 10.2 ± 5.2 | |
| | LD | 44 | 24.9 ± 4.3 | 18.4 ± 3.3 |
| | CH | 21 | (45.5 ± 3.1)[a] | |
| $C_{1.0}SH_{0.8}$ | VLD | 60 | 9.5 ± 3.7 | |
| | LD | 28 | 20.6 ± 3.5 | 13.0 ± 2.8 |
| | CH | 12 | (38.0 ± 3.8)[a] | |
| $C_{1.2}SH_{2.4}$ | VLD | 13 | 7.5 ± 2.0 | |
| | LD | 46.5 | 22.5 ± 4.0 | |
| | CH | 13 | (37.7 ± 2.0)[a] | 19.2 ± 3.2 |
| | CH | 27.5 | (48.0 ± 3.3)[a] | |

[a] Excluded for weighted average calculation.

## 4. Conclusions

Synthesis, drying, and characterization of C–S–H including nanoindentation were performed and presented. The experiments were performed for varying C/S mixture ratios. From TGA, the stoichiometric formulas of the synthetic C–S–H are estimated. The XRDA and $^{29}$Si MAS NMR proved the formation of C–S–H with typical peaks reported in the literature. The silicate polymerization in C–S–H increased with decreasing the C/S ratio. The compaction process was successful for C–S–H synthesized with $C_{1.2}SH_{2.4}$ due to the relatively high water content. Mechanical characterization of the synthetic C–S–H with varying C/S ratios show that while the role of water in enabling good compaction might affect the final stiffness C–S–H, silicate polymerization might also have an effect that becomes apparent for $C_{0.7}SH_{0.6}$. It is evident that there exist some unique differences between the different synthetic C–S–H based on their C/S ratio.

## Acknowledgements

The authors acknowledge funding by US National Science Foundation (NSF) award # 1131369. Financial support to the first author by the Human Resources Development of the Korea Institute of Energy Technology Evaluation and Planning (KETEP) grant funded by the Korea government Ministry of Knowledge Economy (No. 20104010100520) is graciously acknowledged. Technical assistance by Dr. Michael Sheyka with the nanoindentation, Jim Connolly with XRDA, and Professor Karen Smith at University of New Mexico with MAS-NMR are greatly appreciated.

## References

[1] Diamond S. Cement paste microstructure – an overview at several levels. In: Hydraulic cement pastes; their structure and properties. Tapton Hall: University of Sheffield; 1976. p. 2–30.
[2] Beaudoin J, Feldman R. Dependence of degree of silica polymerization and intrinsic mechanical properties of C–S–H on C/S rati. In: 8th International conference on the chemistry of cement, Rio de Janeiro, Brazil; 1986. p. 337–42.
[3] Atkins M, Glasser F, Kindness A. Cement hydrate phases: solubility at 25 °C. Cem Concr Res 1992;22:6.
[4] Sugiyama D. Chemical alteration of calcium silicate hydrate (C–S–H) in sodium chloride solution. Cem Concr Res 2008;38:1270–5.
[5] Alizadeh R, Beaudoin JJ. Mechanical properties of calcium silicate hydrates. Mater Struct 2011;44:13–28.
[6] Feldman R, Ramachandran V. Differentiation of interlayer and adsorbed water in hydrated Portland cement by thermal analysis. Cem Concr Res 1971;1:607–20.
[7] Constantinides G, Ulm F-J, Vliet KV. On the use of nanoindentation for cementitious materials. Mater Struct 2003;36:191–6.
[8] Constantinides G, Ulm F-J. The effect of two types of C–S–H on the elasticity of cement-based materials: results from nanoindentation and micromechanical testing. Cem Concr Res 2004;34:67–80.
[9] Acker P. Micromechanical analysis of creep and shrinkage mechanisms. In: Ulm F, Bazant Z, Wittmann F, editors. Creep, shrinkage, and durability mechanics of concrete and other quasi-brittle materials. Cambridge (MA): Elsevier Science; 2001. p. 15–25.
[10] Mondal P, Shah SP, Marks LD. Nanoscale characterization of cementitious materials. ACI Mater J 2008:174–9.
[11] Taylor HFW. Cement chemistry. 2nd ed. London: Thomas Telford Publishing; 1997.
[12] Thomas J, Jennings H, Allen A. The surface area of cement paste as measured by neutron-scattering-evidence for two C–S–H morphologies. Cem Concr Res 1998;28:897–905.
[13] Young JF, Hansen W. Volume relationships for C–S–H formation based on hydration stoichiometries. In: Strubel L, Brown P, editors. Materials research symposium. Pittsburgh (PA): Materials Research Society; 1987. p. 313–22.
[14] ASTM Standard E 104-02. In: Standard practice for maintaining constant relative humidity by means of aqueous solution. West Conshohocken (PA): ASTM International; 2007. p. 1405–8.
[15] Jain J, Neithalath N. Physico-chemical changes in nano-silica and silica fume modified cement pastes in response to leaching. Int J Mater Struct Integ 2009;3:114–33.
[16] Cong X, Kirkpatrick RJ. $^{29}$Si MAS NMR study of the structure of calcium silicate hydrate. Adv Cem Based Mater 1996;3:144–56.
[17] Saoût GL, Lécolier E, Rivereau A, Zanni H, Chemical structure of cement aged at normal and elevated temperatures and pressures. Part I: Class Goilwell cement. Cem Concr Res 2006;36:71–8.
[18] Taylor HFW. Proposed structure for calcium silicate hydrate gel. J Am Ceram Soc 1986;69:464–7.
[19] Alizadeh R. Nanostructure and engineering properties of basic and modified calcium-silicate-hydrate systems. Ottawa: Department of Civil Engineering, University of Ottawa; 2009. p. 231.
[20] Beaudoin JJ, Raki L, Alizadeh R. A $^{29}$Si MAS NMR study of modified C–S–H nanostructures. Cem Concr Compos 2009;31:585–90.
[21] Kim JJ, Fan T, Reda Taha MM. A homogenization model examining the significance of nanosilica on concrete strength and stiffness. Transportation research record. J Transportation Research Board 2010;V2141:28–35.